Enhanced cycling performance of surface-doped $LiMn_2O_4$ modified by a Li_2CuO_2-Li_2NiO_2 solid solution for rechargeable lithium-ion batteries

Cheng-Gong Han [a], Chunyu Zhu [a*], Genki Saito [a], Nan Sheng [a], Takahiro Nomura [a], Tomohiro Akiyama [a*]

[a] Center for Advanced Research of Energy and Materials, Hokkaido University, Sapporo 060-8628, Japan

[*] Corresponding author: Tel.: +81 11 706 6842, Fax: +81 11 726 0731.

E-mail address: chunyu6zhu@gmail.com (Chunyu Zhu)

takiyama@eng.hokudai.ac.jp (Tomohiro Akiyama)

Abstract

A series of surface-doped $LiMn_2O_4$ samples modified by a Li_2CuO_2-Li_2NiO_2 solid solution were synthesized using a simple and facile sol-gel method to achieve the enhanced cycling performance, especially at elevated temperatures. The corresponding phase structure and morphology were investigated by X-ray diffraction (XRD) and scanning electron microscopy (SEM), respectively. The modified layer on the surface of $LiMn_2O_4$ particles, featuring a $LiNi_\delta Mn_{2-\delta}O_4$-like phase, together with a Li_2CuO_2-Li_2NiO_2 solid solution, as confirmed by XRD and transmission electron microscopy (TEM), plays a key role in alleviating the dissolution of manganese, thus enhancing the cycling performance and rate capability relative to bare $LiMn_2O_4$. The 0.5 wt.%-modified $LiMn_2O_4$ sample delivers a discharge capacity of 113 mAh g^{-1} and a capacity retention of 93.2% following 300 cycles at 1 C and 25 °C, which is higher than the values of 96 mAh g^{-1} and 81.2% for bare $LiMn_2O_4$. In addition, at 55 °C, a capacity retention of 81.2% at 1 C is obtained for the 0.5 wt.%-modified $LiMn_2O_4$ sample after 200 cycles, compared to 70.0% for bare $LiMn_2O_4$. Modifying the surface of the latter by a $LiNi_\delta Mn_{2-\delta}O_4$-like phase mixed with a Li_2CuO_2-Li_2NiO_2 solid solution, is an effective strategy for improving electrochemical properties.

Keywords: $LiMn_2O_4$, cathode, surface modification

1. Introduction

The use of rechargeable Li-ion batteries as a most promising power source for the electric (EVs) and hybrid electric vehicles (HEVs) has attracted increased interest. The cathode material plays a vital role in rechargeable Li-ion batteries owing to its decisive contribution to safety, low cost, and high power/energy densities [1]. Amongst the layered $LiCoO_2$, $LiNiO_2$, $LiNi_{1/3}Co_{1/3}Mn_{1/3}O_2$, and spinel $LiMn_2O_4$ oxide cathode materials, the latter is an attractive and promising candidate due to its low cost, environmental friendliness, abundant resource, easy preparation, high rate capability, and high thermal stability [2–4]. However, $LiMn_2O_4$ often exhibits rapid capacity fading during the charge/discharge process, especially at the elevated temperatures, hindering broad commercial applications. The above problem mainly results from the lattice instability due to the Jahn-Teller effect and the dissolution of lattice manganese in the electrolyte due to the disproportion reaction of Mn^{3+} caused by traces of HF in the electrolyte, with the latter reaction being more important for capacity fading [4–6].

Although cationic doping of Mn sites by Ni^{2+} [7,8], Al^{3+} [9,10], Ru^{4+} [11], Ni-Cu [12], Mg-Si [13], and La-Bi [14], has been carried out to retard capacity fading, the irreversible capacity loss arising from the dissolution of manganese cannot be completely alleviated both at room and elevated temperatures [15]. Surface modification, being another effective approach, is drawing more interest, since it can give rise to improved electrochemical properties due to its protective effect at the cathode/electrolyte interfaces, not only suppressing the dissolution of manganese, but also

improving operation safety and structural stability [16,17]. Many compounds, such as metal oxides [18,19], fluorides [20,21], and phosphates [22,23], have been exploited as surface-modifying materials for upgrading the electrochemical performance of spinel $LiMn_2O_4$. However, these materials often fail to improve the capacity and rate capability owing to the inferior Li^+ migration and/or electron conductivity of the inert layer [24,25]. Recently, modification of $LiMn_2O_4$ by a layer of media containing Li^+ ions and/or electron conductors such as $LiNbO_3$ [1], $LiNi_{0.5}Mn_{1.5}O_4$ [26,27], Li_2ZrO_3 [28], $Li_{1.15}Co_{0.32}Mn_{1.53}O_4$ [29], and $Li_4Ti_5O_{12}$ [30], was used to improve electrochemical properties by accelerating Li ions transport and/or the charge transfer on the surface of the cathode material. Li_2CuO_2, exhibiting an *Immm* orthorhombic phase, possesses a relatively large amount of lithium per unit formula, with the lithium ions located between one-dimensional chains of edge-sharing $[CuO_4]$ square planar units, facilitating rapid transfer of Li^+ ions [31,32]. Li_2CuO_2 delivers a high capacity of 200 mAh g^{-1} and an average discharge voltage of 2.5 V, along with undamaged one-dimensional $[CuO_4]$ chains during cycling [33]. Unfortunately, Li_2CuO_2 exhibits poor lithiation reversibility and a capacity loss during the charge/discharge process [34]. These drawbacks can be retarded by substitution of Cu for Ni, resulting in a Li_2CuO_2-Li_2NiO_2 solid solution due to their isostructure [32,35]. $Li_2Cu_{0.5}Ni_{0.5}O_2$, a solid solution of equivalent amounts of Li_2CuO_2 and Li_2NiO_2 proposed by Imanishi et al. [30], displays a maximum capacity of 250 mAh g^{-1} at a current density of 0.6 mA cm^{-1} in the range of 1.5–4.0 V, together with good reversibility during charge/discharge cycling, as compared with that of pure Li_2CuO_2 and Li_2NiO_2. Ruther et al.

also investigated the structure and electrochemical performance of $Li_2Cu_{0.5}Ni_{0.5}O_2$, which retained its stable structure even after extraction of one lithium per formula unit [36]. A lack of studies on Li_2CuO_2-Li_2NiO_2 solid solutions acting as the surface-modifying materials, appears more important for cathode materials in rechargeable Li-ion batteries based on above merits. On the other hand, surface-doping, i.e., the incorporation of cations into the surface within a depth of several nanometers, has been exploited as an interesting technique to improve cycling performance [37]. $LiMn_2O_4$ modified by a $LiMn_{2-x}Ti_xO_4$ surface layer displays a remarkably improved cycling performance due to the electrochemical activity of the latter, maintaining the ion/charge transport channels on the surface and minimizing the possible phase segregation owing to structural similarity [37]. $LiCu_xMn_{2-x}O_4$-coated $LiMn_2O_4$ exhibits improved electrochemical properties, especially at high current densities, attributed to the significant reduction of side reactions and Mn dissolution at the cathode/electrolyte interface [38]. $LiMn_2O_4$ surface-modified by $LiNi_{0.05}Mn_{1.95}O_4$, prepared by a tartaric acid gel process, exhibits high capacity retention (96%) after 20 cycles, compared to a value of 89% for unmodified $LiMn_2O_4$ at 0.5 C, which is ascribed to the unblocked insertion/extraction of Li [39]. The Ni-doped layer on the surface of $LiMn_2O_4$ particles, is expected to improve their electrochemical performance. Hence, $LiMn_2O_4$ surface-modified with $LiNi_\delta Mn_{1-\delta}O_4$ together with the Li_2CuO_2-Li_2NiO_2 solid solution, was used to improve electrochemical performance.

In this work, solution combustion synthesis (SCS), a highly exothermic and self-sustaining

reaction, was employed to prepare $LiMn_2O_4$ powders, yielding nano-sized particles with high specific areas to facilitate the electrochemical properties [40,41]. The modified $LiMn_2O_4$ samples were prepared by a simple and facile sol-gel method to ensure uniformity of the modified layers. The phase structure, morphology, and electrochemical performance at 25 and 55 °C, were investigated and discussed in detail.

2. Experimental

2.1 Preparation and characterization of surface-doped $LiMn_2O_4$ modified by a Li_2CuO_2-Li_2NiO_2 solid solution.

$LiMn_2O_4$ powders were prepared by SCS with subsequent calcination [41–43]. The following raw materials were used without further purification: lithium nitrate ($LiNO_3$, 99.0%, Kishida Chemical Co., Ltd., Japan), lithium acetate (CH_3COOLi, 99.0%, Kishida Chemical Co., Ltd., Japan), manganese nitrate ($Mn(NO_3)_2$, 50% w/w aqueous solution, Alfa Aesar), nickel nitrate ($Ni(NO_3)_2 \cdot 6H_2O$, 99.9%, Wako Pure Chemical Industries, Ltd., Japan), copper nitrate ($Cu(NO_3)_2 \cdot 3H_2O$, 99.0–104.0%, Wako Pure Chemical Industries, Ltd., Japan), and urea (NH_2CONH_2, 99.0%, Chameleon Reagent, Japan). $LiNO_3$, $Mn(NO_3)_2$ (Li:Mn mole ratio = 1.05:2), and NH_2CONH_2 (φ = 0.5, where φ is the ratio of total valency of urea to total valency of nitrate), were dissolved in distilled water. The homogenous viscous sol-gel formed after evaporating water, was subjected to combustion in a home-made apparatus. The collected powders were subsequently calcined in air at 800 °C for 24 h to obtain $LiMn_2O_4$ powders.

Surface-doped $LiMn_2O_4$ samples modified by a Li_2CuO_2-Li_2NiO_2 solid solution were prepared utilizing a facile sol-gel method. CH_3COOLi, $Ni(NO_3)_2$, and $Cu(NO_3)_2$ were dissolved in distilled water under stirring (in amounts required by equimolar Li_2CuO_2 and Li_2NiO_2) to form a homogenous solution. The obtained solution was dropwise added to an aqueous dispersion of

$LiMn_2O_4$ obtained by ultrasonication. Finally, the modified $LiMn_2O_4$ powders were calcined in air at 600 °C for 3 h. A series of 0, 0.5, 1.0, and 2.0 wt.%-modified samples were prepared, denoted as 0, 0.5, 1.0, and 2.0 wt.% for simplicity, respectively.

Powder X-ray diffraction (XRD, Cu Kα, Rigaku Miniflex600), and scanning electron microscopy (SEM, JEOL, JSM-7001FA) together with transmission electron microscopy (TEM, JEOL, JEM-2010F) were employed to identify the phase structure and characterize the morphology, size, and modified sample layers, respectively. X-ray photoelectron spectroscopy (XPS, JEOL Ltd., JPS-9200) using an Mg Kα X-ray source was used to detect the surface composition.

2.2 Cell assembly and electrochemical measurements.

A Swagelok-type cell was assembled in an Ar-filled glove box [43,44]. The working electrode was prepared by combining 80 wt.% active material, 10 wt.% binder (PVDF) dissolved in N-methyl-2-pyrrolidone (NMP), and 10 wt.% conductive carbon (acetylene black). A lithium metal disk served as the counter and reference electrode. A 1 M lithium hexafluorophosphate ($LiPF_6$) in ethylene carbonate (EC)/dimethyl carbonate (DMC) (1:1 in volume) was used as an electrolyte, and a Celgard polypropylene membrane served as separator. Electrochemical measurements at 25 and 55 °C were galvanostatically conducted in a voltage range of 3.2–4.4 V (at a rate of 1 C, corresponding to the full charge/discharge of 150 mAh g^{-1} in 1 h) using a battery tester (Arbin Instruments, MSTAT4, USA). Cyclic voltammetry (CV) was performed using a

potentiostat/galvanostat (Autolab, PGSTAT128N) in a range of 3.2–4.4 V at a scan rate of 0.1 mV·s^{-1}. Electrochemical impedance spectroscopy (EIS) was conducted employing an Autolab instrument with a frequency response analyzer (FRA), in the frequency range from 1000 kHz to 0.01 Hz.

3. Results and discussion

Figure 1 displays the XRD patterns of modified $LiMn_2O_4$ samples. To monitor the shift of the diffraction peaks after modification, silicon was employed as a reference and calibrant. The diffraction peaks of all samples, except those of silicon, are indexed to the standard spinel $LiMn_2O_4$, belonging to the *Fd*3*m* space group. No diffraction peaks of the Li_2CuO_2-Li_2NiO_2 solid solution are observed, which is ascribed to their low amount and/or amorphous structure [15]. A gradual shift to higher 2θ values is observed for the enlarged diffraction peak of (111) with increasing degree of modification, indicating a shrinking lattice parameter. The lattice parameter and cell volume refined by *MDI Jade* software are shown in Table 1. It is thought that the substitution of Mn^{3+} by Ni^{2+} results in a decreased lattice parameter, mainly due to the stronger Ni-O bonds compared to Mn-O bonds, despite the small difference in the ionic radii of Mn^{3+} (0.65 Å) and Ni^{2+} (0.69 Å) [45–47]. The decreased lattice parameter in this work is deemed to be attributed to the diffusion of a small amount of Ni to the surface of the host spinel particles to form a $LiNi_\delta Mn_{2-\delta}O_4$-like phase, in agreement with the slight shift of the (111) diffraction peak of $LiMn_2O_4$ surface-modified by $LiNi_{0.05}Mn_{1.95}O_4$ to higher 2θ values [39]. On the other hand, we suppose that Cu^{2+} diffuses into the host spinel particles to substitute Mn^{3+}, which is expected to result in an increased lattice parameter due to the larger ionic radius of Cu^{2+} (0.87 Å) compared to that of Mn^{3+} (0.65 Å), coinciding with

the increased lattice parameters of $LiCu_xNi_{2-x}O_4$ coated $LiMn_2O_4$ [38]. The $LiNi_\delta Mn_{2-\delta}O_4$-like phase (detectable by TEM in 2.0 wt.% sample) is produced on the surface of the host spinel particles after the diffusion of a small amount of Ni, not Cu, during calcination at 600 °C for 3 h, benefiting the electrochemical properties.

Figure 2 shows SEM images of modified $LiMn_2O_4$ samples. Primary particles of 200–500 nm size (Fig. 2 inset) agglomerate to form secondary particles with sizes of < 10 μm. The images display similar particle shapes and sizes for all samples, indicating no significant morphology changes after modification. The detection of the modified layers on the surface of $LiMn_2O_4$ particles was performed by TEM images of 0.5 and 2.0 wt.% samples (Fig. 3). A modified layer is invisible on the surface of the 0.5 wt.% sample (Fig. 3 (a)) due to its low amount, whereas that is noticeable on the spinel particle surface for the 2.0 wt.% sample. Interestingly, electron diffraction patterns in the selected area of the modified layer for the 2.0 wt.% sample, were similar but not identical to those of the spinel structure, since the obtained lattice distance of 0.46 nm is slightly lower than the lattice fringe distance of 0.48 nm for the (111) plane of the spinel structure, corresponding to the shift of (111) XRD diffraction peak to higher angles. The above finding is thought to be due to the produced $LiNi_\delta Mn_{2-\delta}O_4$-like phase, not the Li_2CuO_2-Li_2NiO_2 solid solution due to the absence of the characteristic *d*-spacing of around 0.34 nm [36]. The Li_2CuO_2-Li_2NiO_2 solid solution mixed with the $LiNi_\delta Mn_{2-\delta}O_4$-like phase in the modified layer, probably exhibits an amorphous structure based on a number of small modified layer areas with undetectable electron diffraction patterns [43]. In

order to identify the presence of Cu and Ni in the modified layer, the cross section of the 0.5 wt.% sample was characterized by energy dispersive X-ray spectrometry (EDS). The particles were embedded within resin, and the cross section was obtained after mechanical and Ar-ion milling, as shown in Fig. 3 (c). EDS spectra collected from regions 1 (resin) and 2 (resin-particle boundary) (Fig. 3 (d)) is displayed in Fig. 3 (e). The carbon signal originates from the resin, while that of Mo is due to the substrate. Compared with region 1, obvious peaks of Ni and Cu are observed in region 2, indicating the presence of Ni and Cu elements in the surface of the particles.

XPS is always used to determine the surface composition and chemical states of ions. Figure 4 displays the Mn, Cu, Ni $2p_{3/2}$ peaks for 0 and 0.5 wt.% samples. XPS binding energy of Mn $2p_{3/2}$ peaks is located at 642.2 and 642.5 eV for 0 and 0.5 wt.% samples, respectively, which these values are in the range of 614.9 eV (Mn^{3+}) to 642.6 eV (Mn^{4+}) [48,49]. The relative amount of Mn^{4+} is increased from 50.1% for 0 wt.% to 65.1% for 0.5 wt.% sample after splitting Mn $2p_{3/2}$ peak. The more relative amount of Mn^{4+} for 0.5 wt.% will result in a higher average Mn valence of approximately 3.66 than 3.51 for 0 wt.% sample. This can be attributed to the small substitution of Mn by Ni to form $LiNi_{\delta}Mn_{2-\delta}O_4$-like phase, expecting to improve the cycling performance due to increased structure stability. Compared with 0 wt.% sample, 0.5 wt.% sample shows an obvious Cu $2p_{3/2}$ peak located at 933.6–935.2 eV, which is higher than 933.6 eV value (CuO) [50]. The higher Cu $2p_{3/2}$ binding energy was the major XPS characteristic of CuO, indicating the presence of Cu^{2+} at the surface of particles [51,52]. The Ni $2p_{3/2}$ peaks with binding energy of 854.1 eV (NiO) [53] is

hardly observed for the modified sample, which is likely due to a mount of Ni diffusion into the spinel matrix to substitute Mn.

Figure 5 shows the discharge capacity as a function of cycle number for modified $LiMn_2O_4$ samples at 1 C and 25 °C. Bare $LiMn_2O_4$ shows a significantly decreased discharge capacity (96 mAh g^{-1}) with a capacity retention of 81.2% at 1 C after 300 cycles, whereas modified $LiMn_2O_4$ samples exhibit a remarkably enhanced cycling performance. The 0.5, 1.0, and 2.0 wt.% samples deliver discharge capacities of 113, 111, 103 mAh g^{-1}, with capacity retention values of 93.2, 95.0, and 96.3% after 300 cycles, respectively. Moreover, since degree of modification increase in the order of 0.5, 1.0, and 2.0 wt.%, a capacity fading of 0.027, 0.019, 0.013 mAh g^{-1} per cycle is displayed, compared to 0.074 mAh g^{-1} per cycle for bare $LiMn_2O_4$. The improved cycling performance is due to suppressed dissolution of Mn in the electrolyte and the increased stability of the spinel structure after modification.

Figure 6 shows the rate capability of modified $LiMn_2O_4$ samples at 25 °C. An obviously decreased capacity at increased current densities is observed for bare $LiMn_2O_4$, which displays the lowest discharge capacity of 82 mAh g^{-1} among all samples at 7 C. This can be rationalized by the great battery polarization resulting from the limited Li-ion diffusion during cycling, as compared to the modified samples [54]. In particular, the 0.5 wt.% sample delivers the best rate capability, showing a discharge capacity of 120 mAh g^{-1} at 1 C, 115 mA hg^{-1} at 2 C, 111 mAh g^{-1} at 3 C, 107 mAh g^{-1} at 4 C, 103 mAh g^{-1} at 5 C, and 95 mAh g^{-1} at 7 C. Compared to bare $LiMn_2O_4$, the above

sample recovers its high capacity after discharging at 7 C and displays a smaller capacity difference between 1 to 2 C. The capacity retention (relative to 1 C) is increased in the order of 0 wt.% < 0.5 wt.% < 1.0 wt.% < 2.0 wt.% at the corresponding current densities. This increased capacity retention of modified samples indicates higher lithium and/or electron conductivity compared with the bare $LiMn_2O_4$.

High electrochemical performance at elevated temperatures is critical for commercial usage of spinel $LiMn_2O_4$ cathodes in rechargeable Li-ion batteries. Figure 7 displays the dependence of discharge capacity on the number of cycles for modified $LiMn_2O_4$ samples at 1 C and 55 °C. Bare $LiMn_2O_4$ displays a significantly decreased capacity after cycling at 1 C and 55 °C, maintaining a discharge capacity of only 83 mAh g^{-1} after 200 cycles. A remarkably enhanced cycling performance is achieved for the modified $LiMn_2O_4$ samples. Improved capacity retention values of 81.2, 81.2, and 92.2% after 200 cycles are obtained for 0.5, 1.0, and 2.0 wt.% samples, respectively, compared to the value of 70.0% for bare $LiMn_2O_4$. These higher capacity retentions at 55 °C and 1 C, than 80% of $LiNi_{0.2}Mn_{1.8}O_4$ at 60 °C and 0.1 C after 100 cycles [8], confirm the cycling stability of modified $LiMn_2O_4$. An improved capacity retention at 55 °C, which is coinciding with that at 25 °C, is observed for the higher degrees of modification that result in a lesser extent of manganese dissolution and more stable spinel structure, thereby enhancing cycling performance [43].

Figure 8 shows the charge-discharge curves of modified $LiMn_2O_4$ samples at 1 C and 55 °C. Two obvious plateaus are observed for all samples, indicating two oxidation/reduction reactions during

Li extraction/insertion. The plateaus at 4.0–4.1, and 3.9–4.0 V, correspond to the $MnO_2/Li_{0.5}Mn_2O_4$, and $Li_{0.5}Mn_2O_4/LiMn_2O_4$ phase transitions, respectively [55,56]. A small voltage difference between the charge and discharge plateaus is obtained for the modified samples in comparison with bare $LiMn_2O_4$, indicating smaller battery polarization [27]. The modified $LiMn_2O_4$ samples exhibit a smaller initial capacity loss after 200 cycles and better cycling performance.

In order to clearly understand the oxidation/reduction of cathode materials during cycling, CV curves of modified $LiMn_2O_4$ samples were recorded (Fig. 9). Two pairs of peaks, corresponding to the two charge-discharge plateaus in Fig. 8, indicate two reversible redox reactions during Li extraction/insertion. The unchanged CV curves of the modified samples, as compared with those of bare $LiMn_2O_4$, confirm that modification does not affect the electrochemical process of spinel $LiMn_2O_4$. The potential values of the first CV curve cycle are shown in Table 2. The 0.5, 1.0, and 2.0 wt.% samples exhibit higher cathodic peaks of 3.96/4.07, 3.96/4.08, and 3.97/4.10 V, respectively, than bare $LiMn_2O_4$ (3.93/4.06 V). This indicates that the modified samples can supply an improved operating voltage during the discharge process in comparison with the unmodified $LiMn_2O_4$. Note that ΔE_p is the potential difference between the anodic (E_{pa}) and cathodic (E_{pc}) peaks. The values of E_{p1}/E_{P2} decrease in the order of 0 wt.% > 0.5 wt.% > 1.0 wt.% > 2.0 wt.%, being equal to 0.14/0.14, 0.12/0.14, 0.12/0.12, and 0.08/0.08 V, respectively. These values indicate a weaker polarization and easier extraction/insertion of Li ions for the modified samples [57]. The modified material can alleviate the dissolution of Mn and preserve the stable structure of the spinel

$LiMn_2O_4$ during Li extraction/insertion.

The rate capability of 0 and 0.5 wt.% samples at 55 °C is shown in Fig. 10 (a). Compared with bare $LiMn_2O_4$, the modified sample exhibits improved rate capability at high temperature. The 0.5 wt.% sample delivers a high discharge capacity of 96 mAh g^{-1} and a capacity retention of 78.7% (relative to 1 C), compared with the respective values of 89 mAh g^{-1} and 71.4% for the 0 wt.% sample at 7 C. The former sample exhibits a lesser capacity fading than bare $LiMn_2O_4$ at 1, 2, and 3 C, together with that at 1 and 2 C in recovered stage after 60 cycles. This indicates that the modifying material can effectively suppress the dissolution of manganese and preserve structural stability even at high temperature. Figure 10 (b) shows the discharge curves of the first cycle at different current densities for 0 and 0.5 wt.% samples at 55 °C. The solid line corresponds to the 0.5 wt.% sample, while the dished line represents the 0 wt.% sample. Compared to bare $LiMn_2O_4$, the modified sample still delivers similar high voltages at different current densities, indicating that modification can result in unimpaired voltage during the discharge process. The above voltage is decreased with increasing current densities. The shape of the discharge curves gradually transforms from two obvious plateaus at 1, 2, and 3 C into a slopping line at 4, 5, and 7 C, demonstrating the ohmic drop and increased cell polarization at high current densities [58].

EIS is an important tool to investigate the electrochemical properties of electrodes. Figure 11 displays the Nyquist plots of modified $LiMn_2O_4$ samples after 200 cycles at 1 C and 55 °C, along with the equivalent circuit in the inset used to fit the spectra. As shown in the equivalent circuit, R_S

is the ohmic resistance that includes electrolyte and electrode resistance, R_f represents the resistance of Li-ion diffusion in the surface layer (solid electrolyte interphase (SEI) film and modified layer), and R_{ct} is the charge transfer resistance. Constant phase elements, CPE_1 and CPE_2, denote the capacitance of the SEI film and the double layer, respectively. CPE_3 is chosen instead of the finite Warburg element to properly fit the Nyquist plots in the low-frequency region [59]. The EIS data simulated by *Zsimpwin* software are listed in Table 3. A large R_f value of 27.01 Ω and R_{ct} value of 75.60 Ω are obtained for bare $LiMn_2O_4$, decreasing after the modification. The decreased R_f and R_{ct} values indicate that the modified layer can alleviate the side reactions at the electrode/electrolyte interface to improve the cycling performance by suppressing SEI film formation and enhancing charge transport [60]. In particular, the lowest R_f and R_{ct} values of 6.54 and 49.23 Ω are achieved for the 0.5 wt.% sample. As the degree of modification increases, so do R_f, and R_{ct}, which is consistent with our previous report and can be attributed to the dominant role of hindered Li-ion diffusion via the thick modified layer due to the increased Li-ion diffusion path, regardless of the enhanced Li-ion diffusion via the retarded SEI film [43].

To detect the effect of the modified layer on the structural stability of spinel $LiMn_2O_4$, an investigation of the cycled electrode morphology was carried out. Figure 12 displays SEM images of the cycled electrodes for 0 and 0.5 wt.% samples, before cycling (a) and (b), and after 300 cycling (c) and (d) at 1 C and 25 °C, respectively. Compared to Fig. 12 (a), an obvious large crevice, along with the small crevice on the particles shown in the inset, is observed after 300 cycles for the

0 wt.% sample in Fig. 12 (c), arising from the erosion by HF in the electrolyte and the inferior stability of the spinel structure [61]. No morphology changes are noticed for the 0.5 wt.% sample before cycling (Fig.11 (b)) and after 300 cycles (Fig. 12 (d)), reflecting the fact that the protective modified layer can restrain the electrolyte erosion and preserve structural stability, resulting in improved cycling performance.

4. Conclusions

Surface-doped $LiMn_2O_4$ modified by a solid solution of Li_2CuO_2-Li_2NiO_2 was synthesized by a simple and facile sol-gel method. XRD and SEM confirmed the presence of a $LiNi_\delta Mn_{2-\delta}O_4$-like phase (detectable by TEM), and the similar morphology, respectively. The electrochemical properties at 25 and 55 °C, in particular the cycling performance, were improved for the modified $LiMn_2O_4$ samples. Following 300 cycles at 25 °C, a high capacity retention of 93.2% and a discharge capacity of 113 mAh g^{-1}, were delivered by the 0.5 wt.% sample at 1 C, compared with the respective values of 81.2% and 96 mAh g^{-1} for the bare $LiMn_2O_4$. After 200 cycles at 55 °C, a remarkably improved capacity retention of 81.2% was exhibited by the 0.5 wt.% sample, being higher than the value of 70.0% for bare $LiMn_2O_4$ at 1 C. The enhanced cycling performance is attributed to the modified layer, which acts as a protecting medium to suppress the dissolution of manganese and support the structural stability, along with the intrinsic character of allowing the effective mobility of Li ions. The $LiNi_\delta Mn_{2-\delta}O_4$-like phase together with the Li_2CuO_2-Li_2NiO_2 solid solution can be considered appropriate candidates for surface modification to obtain enhanced electrochemical properties of spinel $LiMn_2O_4$.

Acknowledgements

This work was partially supported by the Japan Society for Promotion of Science (JSPS) and the Japan Science and Technology Agency (JST). We thanks “Nanotechnology Platform” Program of the Ministry of Education for allowing us to use TEM. Cheng-Gong Han also acknowledges the scholarship from the China Scholarship Council (CSC).

Reference

[1] Z.-J. Zhang, S.-L. Chou, Q.-F. Gu, H.-K. Liu, H.-J. Li, K. Ozawa, J.-Z. Wang, Enhancing the high rate capability and cycling stability of $LiMn_2O_4$ by coating of solid-state electrolyte $LiNbO_3$, ACS Appl. Mater. Interfaces 6 (2014) 22155.

[2] A. Yamada, M. Tanaka, Jahn-Teller structural phase-transition around 280 K in $LiMn_2O_4$, Mater. Res. Bull. 30 (1995) 715.

[3] O.K. Park, Y. Cho, S. Lee, H.-C. Yoo, H.-K. Song, J. Cho, Who will drive electric vehicles, olivine or spinel?, Energy Environ. Sci. 4 (2011) 1621.

[4] Y.Y. Xia, Y.H. Zhou, M. Yoshio, Capacity fading on cycling of 4 V $Li/LiMn_2O_4$ cells, J. Electrochem. Soc. 144 (1997) 2593.

[5] R.J. Gummow, A. Dekock, M.M. Thackeray, Improved capacity retention in rechargeable 4 V lithium lithium manganese oxide (spinel) cells, Solid State Ionics 69 (1994) 59.

[6] W. Choi, A. Manthiram, Comparison of metal ion dissolutions from lithium ion battery cathodes, J. Electrochem. Soc. 153 (2006) A1760.

[7] H.M. Wu, J.P. Tu, X.T. Chen, Y. Li, X.B. Zhao, G.S. Cao, Effects of Ni-ion doping on electrochemical characteristics of spinel $LiMn_2O_4$ powders prepared by a spray-drying method, J. Solid State Electrochem. 11 (2007) 173.

[8] K. Raju, F.P. Nkosi, E. Viswanathan, M.K. Mathe, K. Damodaranc, K.I. Ozoemena, Microwave-enhanced electrochemical cycling performance of the $LiNi_{0.2}Mn_{1.8}O_4$ spinel cathode material at elevated temperature, Phys. Chem. Chem. Phys., 18 (2016) 13074.

[9] F.P. Nkosi, C.J. Jafta, M. Kebede, L. Roux, M. K. Mathe, K.I. Ozoemena, Microwave-assisted optimization of the manganese redox states for enhanced capacity and capacity retention of $LiAl_xMn_{2-x}O_4$ (x = 0 and 0.3) spinel materials, RSC Adv., 5 (2015) 32256.

[10] A.B. Yuan, L. Tian, W.M. Xu, Y.Q. Wang, Al-doped spinel $LiAl_{0.1}Mn_{1.9}O_4$ with improved high-rate cyclability in aqueous electrolyte, J. Power Sources 195 (2010) 5032.

[11] H.L. Wang, T.A. Tan, P. Yang, M.O. Lai, L. Lui, High-rate performances of the Ru-doped spinel $LiNi_{0.5}Mn_{1.5}O_4$: effects of doping and particle size, J. Phys. Chem. C 115 (2011) 6102.

[12] M.C. Yang, B. Xu, J.H. Cheng, C.J. Pan, B.J. Hwang, Y.S. Meng, Electronic, structural, and electrochemical properties of $LiNi_xCu_yMn_{2-x-y}O_4$ ($0 < x < 0.5$, $0 < y < 0.5$) high-voltage spinel materials, Chem. Mater. 23 (2011) 2832.

[13] H. Zhao, F. Li, X. Liu, C. Cheng, Z. Zhang, Y. Wu, W. Xiong, B. Chen, Effects of equimolar Mg (II) and Si (IV)

co-doping on the electrochemical properties of spinel $LiMn_{2-2x}Mg_xSi_xO_4$ prepared by citric acid assisted sol–gel method, Electrochim. Acta 151 (2015) 263.

[14] C.-G. Han, C. Zhu, G. Saito, T. Akiyama, Improved electrochemical properties of $LiMn_2O_4$ with the Bi and La co-doping for lithium-ion batteries, RSC Adv. 5 (2015) 73315.

[15] H. Ming, Y. Yan, J. Ming, J. Adkins, X. Li, Q. Zhou, J. Zheng, Gradient V_2O_5 surface-coated $LiMn_2O_4$ cathode towards enhanced performance in Li-ion battery applications, Electrochim. Acta 120 (2014) 390.

[16] T.-F. Yi, Y.-R. Zhu, X.-D. Zhu, J. Shu, C.-B. Yue, A.-N. Zhou, A review of recent developments in the surface modification of $LiMn_2O_4$ as cathode material of power lithium-ion battery, Ionics 15 (2009) 779.

[17] C.M. Julien, A. Mauger, H. Groult, K. Zaghib, Surface modification of positive electrode materials for lithium-ion batteries, Thin Solid Films 572 (2014) 200.

[18] M. Michalska, B. Hamankiewicz, D. Ziółkowska, M. Krajewski, L. Lipińska, M. Andrzejczuk, A. Czerwiński, Influence of $LiMn_2O_4$ modification with CeO_2 on electrode performance, Electrochim. Acta 136 (2014) 286.

[19] W.-K. Kim, D.-W. Han, W.-H. Ryu, S.-J. Lim, H.-S. Kwon, Al_2O_3 coating on $LiMn_2O_4$ by electrostatic attraction forces and its effects on the high temperature cyclic performance, Electrochim. Acta 71 (2012) 17.

[20] A. Tron, Y.D. Park, J. Mun, AlF_3-coated $LiMn_2O_4$ as cathode material for aqueous rechargeable lithium battery with improved cycling stability, J. Power Sources 325 (2016) 360.

[21] Q. Chen, Y. Wang, T. Zhang, W. Yin, J. Yang, X. Wang, Electrochemical performance of LaF_3-coated $LiMn_2O_4$ cathode materials for lithium ion batteries, Electrochim. Acta 83 (2012) 65.

[22] C. Qing, Y. Bai, J. Yang, W. Zhang, Enhanced cycling stability of $LiMn_2O_4$ cathode by amorphous $FePO_4$ coating, Electrochim. Acta 56 (2011) 6612.

[23] Y. Shang, J. Liu, T. Huang, A. Yu, Effect of heat treatment on the structure and electrochemical performance of $FePO_4$ coated spinel $LiMn_2O_4$, Electrochim. Acta 113 (2013) 248.

[24] Y. Chen, K. Xie, C. Zheng, Z. Ma, Z. Chen, Enhanced Li storage performance of $LiNi_{0.5}Mn_{1.5}O_4$–coated $0.4Li_2MnO_3{\cdot}0.6LiNi_{1/3}Co_{1/3}Mn_{1/3}O_2$ cathode materials for Li-ion batteries, ACS Appl. Mater. Interfaces 6 (2014) 16888.

[25] J. Zhang, H. Zhang, R. Gao, Z. Li, Z. Hu, X. Liu, New insights into the modification mechanism of Li-rich $Li_{1.2}Mn_{0.6}Ni_{0.2}O_2$ coated by Li_2ZrO_3, Phys. Chem. Chem. Phys. 18 (2016) 13322.

[26] T. Qiu, J. Wang, Y. Lu, W. Yang, Improved elevated temperature performance of commercial $LiMn_2O_4$ coated with $LiNi_{0.5}Mn_{1.5}O_4$, Electrochim. Acta 147 (2014) 626.

[27] Z. Han, X. Jia, H. Zhan, Y. Zhou, $LiMn_2O_4$/$LiNi_{0.5}Mn_{1.5}O_4$ composite with improved electrochemical property, Electrochim. Acta 114 (2013) 772.

[28] X. Yi, X. Wang, B. Ju, H. Shu, W. Wen, R. Yu, D. Wang, X. Yang, Effective enhancement of electrochemical performance for spherical spinel $LiMn_2O_4$ via Li ion conductive Li_2ZrO_3 coating, Electrochim. Acta 134 (2014) 143.

[29] M. Jeong, M.-J. Lee, J. Cho, S. Lee, Surface Mn oxidation state controlled spinel $LiMn_2O_4$ as a cathode material for high-energy Li-ion batteries, Adv. Energy Mater. 5 (2015) 1500440.

[30] D.-Q. Liu, X.-Q. Liu, Z.-Z. He, The elevated temperature performance of $LiMn_2O_4$ coated with $Li_4Ti_5O_{12}$ for lithium ion battery, Mater. Chem. Phys. 105 (2007) 362.

[31] F. Sapiña, J. Rodríguez-Carvajal, M.J. Sanchis, R. Ibáñez, A. Beltrán, D. Beltrán, Crystal and magnetic structure of Li_2CuO_2, Solid State Commun. 74 (1990) 779.

[32] N. Imanishi, K. Shizuka, T. Ikenishi, T. Matsumura, A. Hirano, Y. Takeda, Preparation and electrochemical properties of a Li_2CuO_2–Li_2NiO_2 solid solution as a lithium-intercalation electrode, Solid State Ionics 177 (2006) 1341.

[33] H. Arai, S. Okada, Y. Sakurai, J.-i. Yamaki, Electrochemical and structural study of Li_2CuO_2, $LiCuO_2$ and $NaCuO_2$, Solid State Ionics 106 (1998) 45.

[34] C.T. Love, W. Dmowski, M.D. Johannes, K.E. Swider-Lyons, Structural originations of irreversible capacity loss from highly lithiated copper oxides, J. Solid State Chem. 184 (2011) 2412.

[35] E. Setiawati, M. Hayashi, M. Tsuda, K. Hayashi, R. Kobayashi, Structural changes and electrochemical properties of $Li_2Cu_{1-x}M_xO_2$ for lithium secondary batteries, Solid State Ionics 262 (2014) 115.

[36] R.E. Ruther, H. Zhou, C. Dhital, K. Saravanan, A.K. Kercher, G. Chen, A. Huq, F.M. Delnick, J. Nanda, Synthesis, structure, and electrochemical performance of high capacity $Li_2Cu_{0.5}Ni_{0.5}O_2$ cathodes, Chem. Mater. 27 (2015) 6746.

[37] J. Lu, C. Zhan, T. Wu, J. Wen, Y. Lei, A.J. Kropf, H. Wu, D.J. Miller, J.W. Elam, Y.-K. Sun, X. Qiu, K. Amine, Effectively suppressing dissolution of manganese from spinel lithium manganate via a nanoscale surface-doping approach, Nat. Commun. 5 (2014) 5693.

[38] H.W. Chan, J.G. Duh, S.R. Sheen, S.Y. Tsai, C.R. Lee, New surface modified material for $LiMn_2O_4$ cathode material in Li-ion battery, Surf. Coat. Technol. 200 (2005) 1330.

[39] Y.F. Yuan, H.M. Wu, S.Y. Guo, J.B. Wu, J.L. Yang, X.L. Wang, J.P. Tu, Preparation, characteristics and electrochemical properties of surface-modified $LiMn_2O_4$ by doped $LiNi_{0.05}Mn_{1.95}O_4$, Appl. Surf. Sci. 255 (2008) 2225.

[40] A.S. Mukasyan, P. Dinka, Novel approaches to solution-combustion of nanomaterials, Int. J. Self-Propag. High-Temp Synth. 16 (2007) 23.

[41] C.-G. Han, C. Zhu, G. Saito, T. Akiyama, Glycine/sucrose-based solution combustion synthesis of high-purity $LiMn_2O_4$ with improved yield as cathode materials for lithium-ion batteries, Adv. Powder Technol. 26 (2015) 665.

[42] C. Zhu, A. Nobuta, G. Saito, I. Nakatsugawa, T. Akiyama, Solution combustion synthesis of $LiMn_2O_4$ fine powders for lithium ion batteries. Adv. Powder Technol. 25 (2014) 342.

[43] C.-G. Han, C. Zhu, G. Saito, T. Akiyama, Improved electrochemical performance of $LiMn_2O_4$ surface-modified by a Mn^{4+}-rich phase for rechargeable lithium-ion batteries, Electrochim. Acta 209 (2016) 225.

[44] C. Zhu, G. Saito, T. Akiyama, A new $CaCO_3$-template method to synthesize nanoporous manganese oxide hollow structures and their transformation to high-performance $LiMn_2O_4$ cathodes for lithium-ion batteries, J. Mater. Chem. A 1 (2013) 7007.

[45] H. Berg, J.O. Thomas, W. Liu, G.C. Farrington, A neutron diffraction study of Ni substituted $LiMn_2O_4$, Solid State Ionics 112 (1998) 165.

[46] Y.J. Wei, L.Y. Yan, C.Z. Wang, X.G. Xu, F. Wu, G. Chen, Effects of Ni doping on MnO_6 octahedron in $LiMn_2O_4$, J. Phys. Chem. B 108 (2004) 18547.

[47] M.G. Lazarraga, L. Pascual, H. Gadjov, D. Kovacheva, K. Petrov, J.M. Amarilla, R.M. Rojas, M.A. Martin-Luengo,

J.M. Rojo, Nanosize $LiNi_yMn_{2-y}O_4$ ($0 < y \leq 0.5$) spinels synthesized by a sucrose-aided combustion method. characterization and electrochemical performance, J. Mater. Chem. 14 (2004) 1640.

[48] V. Di Castro, G. Polzonetti, XPS study of MnO oxidation, J. Electron. Spectrosc. Relat. Phenom. 48 (1989) 117.

[49] H.W. Nesbitt, D. Banerjee, Interpretation of XPS Mn(2p) spectra of Mn oxyhydroxides and constraints on the mechanism of MnO_2 precipitation, Am. Mineral. 83 (1998) 305.

[50] S. Poulston, P.M. Parlett, P. Stone, M. Bowker, Surface oxidation and reduction of CuO and Cu_2O studied using XPS and XAES, Surf. Interface Anal. 24 (1996) 811.

[51] Y. Wang, F. Qu, J. Liu, Y. Wang, J. Zhou, S. Ruan, Enhanced H_2S sensing characteristics of CuO-NiO core-shell microspheres sensors, Sens. Actuators, B: Chem. 209 (2015) 515.

[52] X. Ma, X. Feng, X. He, H. Guo, L. Lv, J. Guo, H. Cao, T. Zhou, Mesoporous CuO/CeO_2 bimetal oxides: one-pot synthesis, characterization and their application in catalytic destruction of 1,2-dichlorobenzene, Microporous Mesoporous Mater. 158 (2012) 214.

[53] S.H. Kang, J. Kim, M.E. Stoll, D. Abraham, Y.K. Sun, K. Amine, Layered $Li(Ni_{0.5-x}Mn_{0.5-x}M_{2x}')O_2$ (M′ = Co, Al, Ti; $x = 0$, 0.025) cathode materials for Li-ion rechargeable batteries, J. Power Sources 112 (2002) 41.

[54] W. Wen, B. Ju, X. Wang, C. Wu, H. Shu, X. Yang, Effects of magnesium and fluorine co-doping on the structural and electrochemical performance of the spinel $LiMn_2O_4$ cathode materials, Electrochim. Acta 147 (2014) 271.

[55] P. Mohan, B. Ranjith, G.P. Kalaignan, Structure and electrochemical performances of co-substituted $LiSm_xLa_{0.2-x}Mn_{1.80}O_4$ cathode materials for rechargeable lithium-ion batteries, J. Solid State Electrochem. 18 (2014) 2183.

[56] Y.L. Ding, J.A. Xie, G.S. Cao, T.J. Zhu, H.M. Yu, X.B. Zhao, Single-crystalline $LiMn_2O_4$ nanotubes synthesized via template-engaged reaction as cathodes for high-power lithium ion batteries, Adv. Funct. Mater. 21 (2011) 348.

[57] A. Iqbal, Y. Iqbal, L. Chang, S. Ahmed, Z.Y. Tang, Y. Gao, Enhanced electrochemical performance of La- and Zn-co-doped $LiMn_2O_4$ spinel as the cathode material for lithium-ion batteries, J. Nanopart. Res. 14 (2012) 1206.

[58] Y.L. Ding, J. Xie, G.S. Cao, T.J. Zhu, H.M. Yu, X.B. Zhao, Enhanced elevated-temperature performance of Al-doped single-crystalline $LiMn_2O_4$ nanotubes as cathodes for lithium ion batteries, J. Phys. Chem. C. 115 (2011) 9821.

[59] Q.-C. Zhuang, T. Wei, L.-L. Du, Y.-L. Cui, L. Fang, S.-G. Sun, An electrochemical impedance spectroscopic study of the electronic and ionic transport properties of spinet $LiMn_2O_4$, J. Phys. Chem. C. 114 (2010) 8614.

[60] X. Bian, Q. Fu, X. Bie, P. Yang, H. Qiu, Q. Pang, G. Chen, F. Du, Y. Wei, Improved electrochemical performance and thermal stability of Li-excess $Li_{1.18}Co_{0.15}Ni_{0.15}Mn_{0.52}O_2$ cathode material by Li_3PO_4 surface coating, Electrochim. Acta 174 (2015) 875.

[61] N. Wu, H. Wu, H. Liu, Y. Zhang, Solvothermal coating $LiNi_{0.8}Co_{0.15}Al_{0.05}O_2$ microspheres with nanoscale Li_2TiO_3 shell for long lifespan Li-ion battery cathode materials, J. Alloys Compd. 665 (2016) 48.

Figure captions

Fig. 1 XRD patterns of modified $LiMn_2O_4$ samples.

Fig. 2 SEM images of modified $LiMn_2O_4$ samples.

Fig. 3 TEM images of 0.5 wt.% (a), and 2.0 wt.% (b) sample, the schematic of cross section (c), TEM image of cross section for 0.5 wt.% sample (d), EDS of region 1 and 2 (e).

Fig. 4 XPS of Mn, Cu, Ni $2p_{3/2}$ peaks for 0 wt.% and 0.5 wt.% samples.

Fig. 5 Discharge capacity vs. cycle number for modified $LiMn_2O_4$ samples at 1 C and 25 °C.

Fig. 6 Rate capability of modified $LiMn_2O_4$ samples at 25 °C.

Fig. 7 Discharge capacity vs. cycle number for modified $LiMn_2O_4$ samples at 1 C and 55 °C.

Fig. 8 Charge-discharge curves of modified $LiMn_2O_4$ samples at 1 C and 55 °C.

Fig. 9 CV curves of modified $LiMn_2O_4$ samples.

Fig. 10 Rate capability (a), and discharge curves (b) for 0 wt.% and 0.5 wt.% samples at 55 °C.

Fig. 11 EIS of modified $LiMn_2O_4$ samples after the 200 cycles at 1 C and 55 °C.

Fig. 12 SEM of the cycled electrodes for 0 wt.%, and 0.5 wt.% samples, (a) and (b) before cycling, (c) and (d) after 300 cycling at 1 C and 25 °C , respectively.

Fig. 1

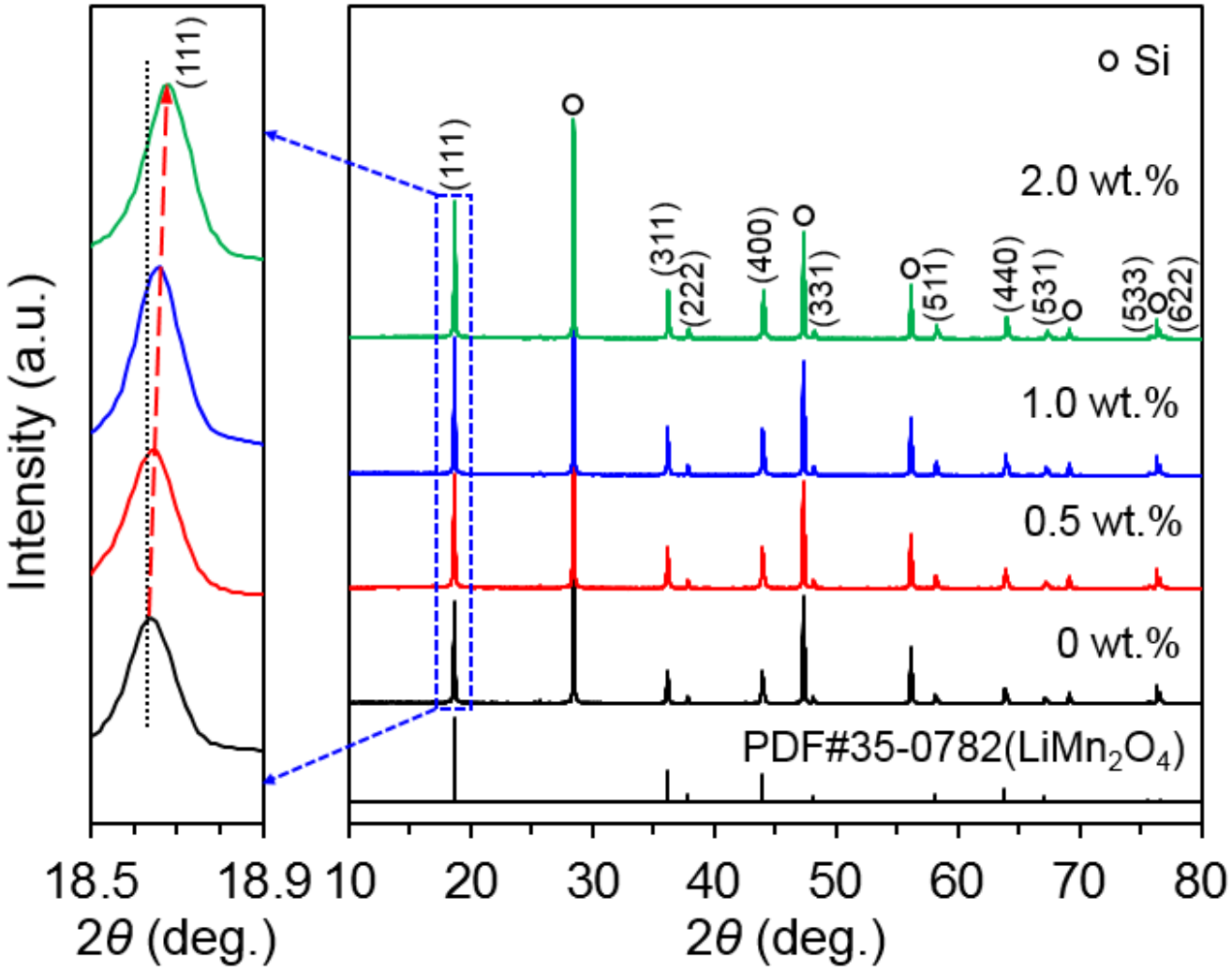
Intensity (a.u.)
(111)
o Si
2.0 wt.%
1.0 wt.%
0.5 wt.%
0 wt.%
PDF#35-0782(LiMn2O4)
(111)
(311)
(222)
(400)
(331)
(511)
(440)
(531)
(533)
(622)
18.5
18.9
10
20
30
40
50
60
70
80
2θ (deg.)
2θ (deg.)

Fig. 2

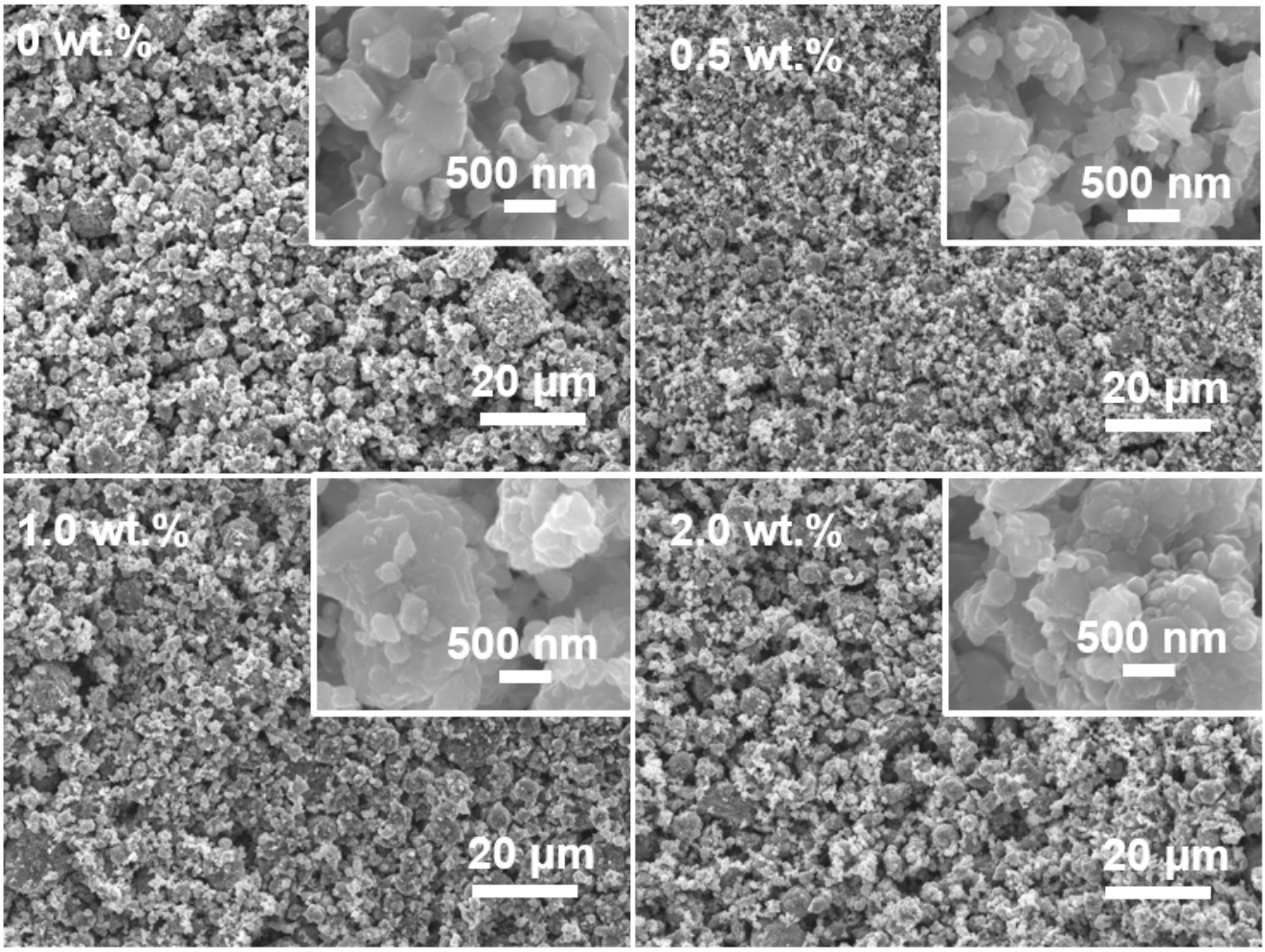
0 wt.%
500 nm
20 µm
0.5 wt.%
500 nm
20 µm
1.0 wt.%
500 nm
20 µm
2.0 wt.%
500 nm
20 µm

Fig. 3

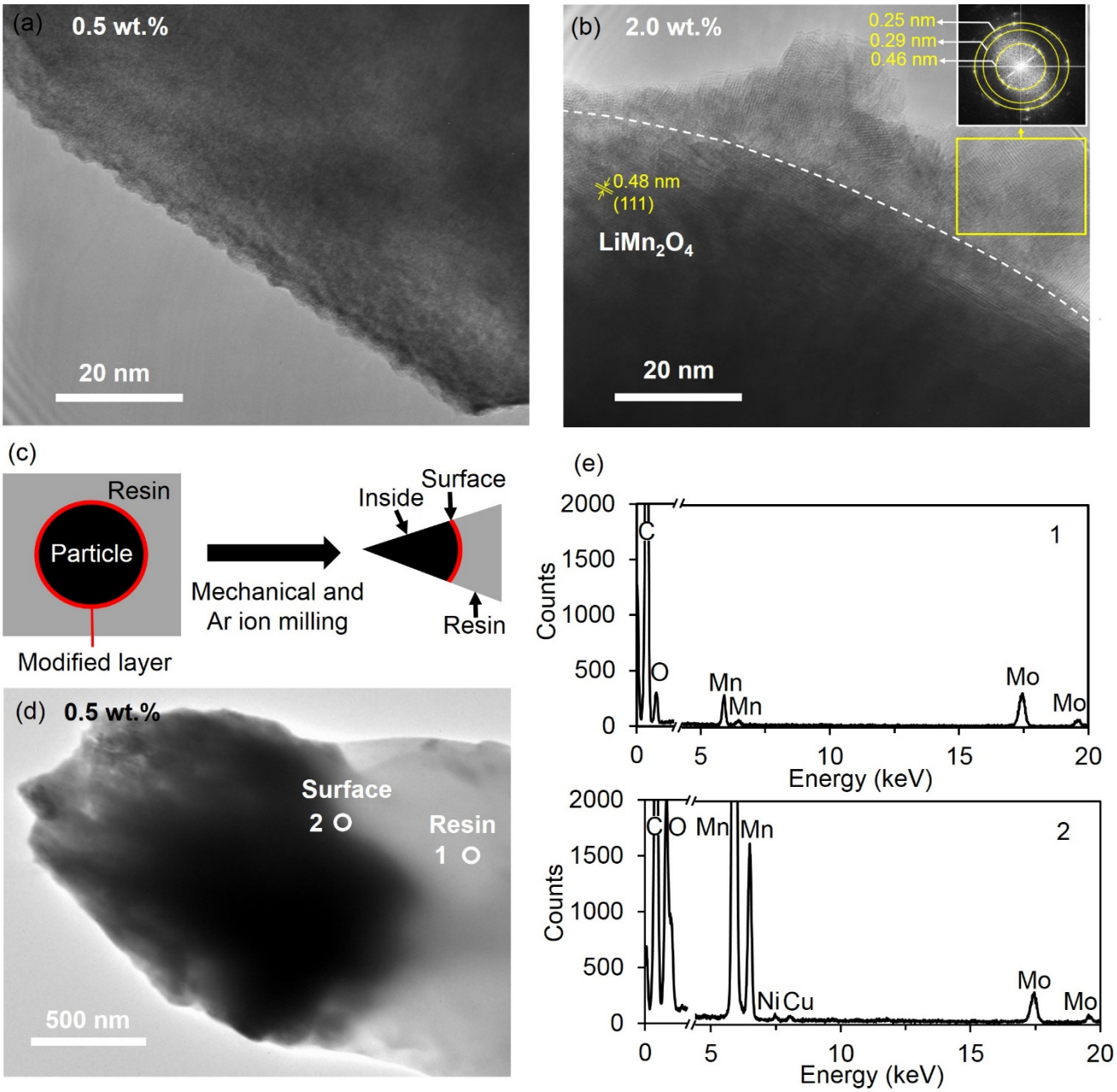
(a) 0.5 wt.%
20 nm
(b) 2.0 wt.%
0.25 nm
0.29 nm
0.46 nm
0.48 nm
(111)
LiMn2O4
20 nm
(c)
Resin
Particle
Modified layer
Mechanical and
Ar ion milling
Surface
Inside
Resin
(d) 0.5 wt.%
Surface
2
Resin
1
500 nm
(e)
Counts
Energy (keV)
C
O
Mn
Mn
Mo
Mo
1
Ni
Cu
2

Fig. 4

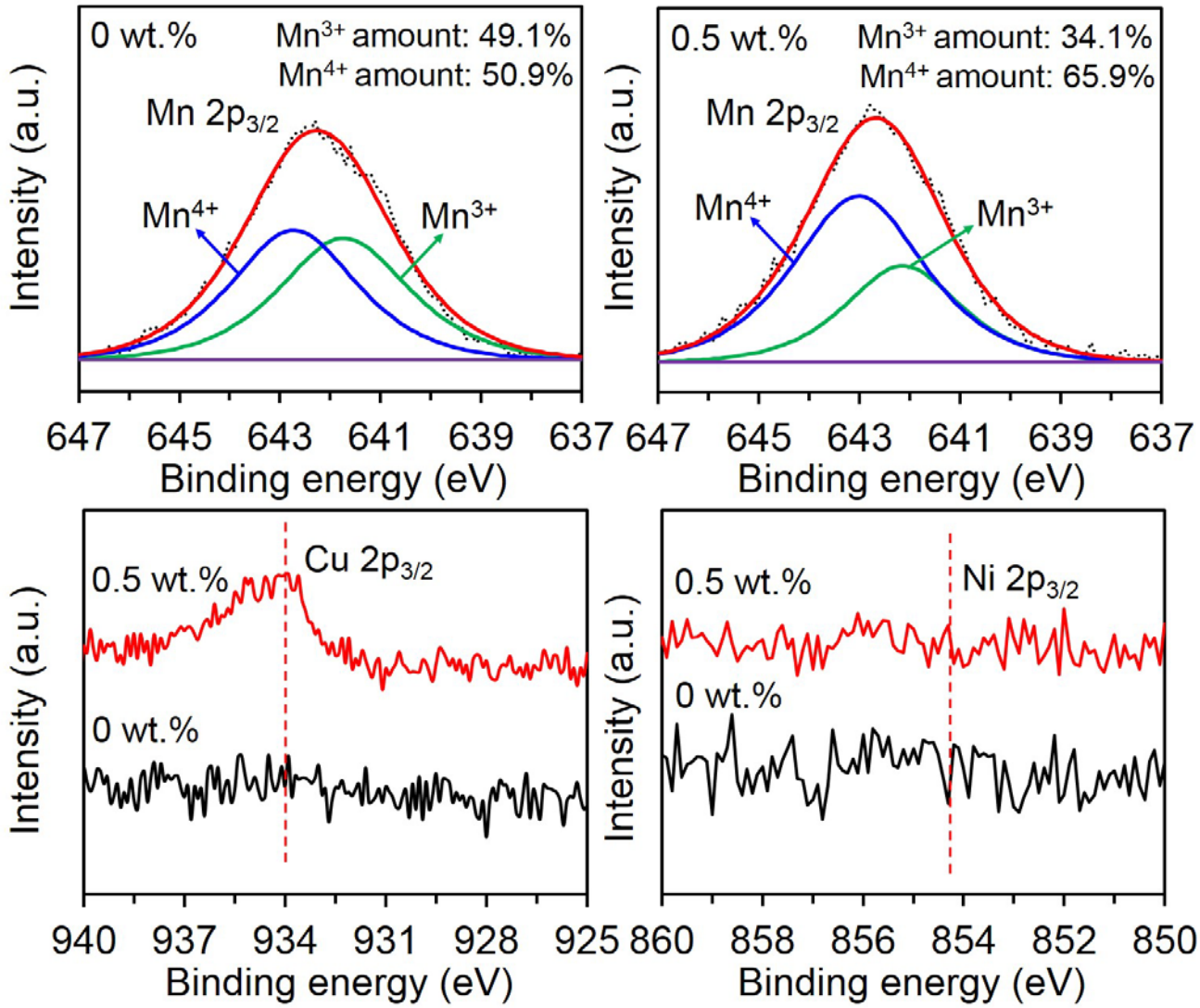
0 wt.%
Mn3+ amount: 49.1%
Mn4+ amount: 50.9%
Mn 2p3/2
Mn4+
Mn3+
Intensity (a.u.)
647 645 643 641 639 637
Binding energy (eV)
0.5 wt.%
Mn3+ amount: 34.1%
Mn4+ amount: 65.9%
Mn 2p3/2
Mn4+
Mn3+
Intensity (a.u.)
647 645 643 641 639 637
Binding energy (eV)
0.5 wt.%
Cu 2p3/2
0 wt.%
Intensity (a.u.)
940 937 934 931 928 925
Binding energy (eV)
0.5 wt.%
Ni 2p3/2
0 wt.%
Intensity (a.u.)
860 858 856 854 852 850
Binding energy (eV)

Fig. 5

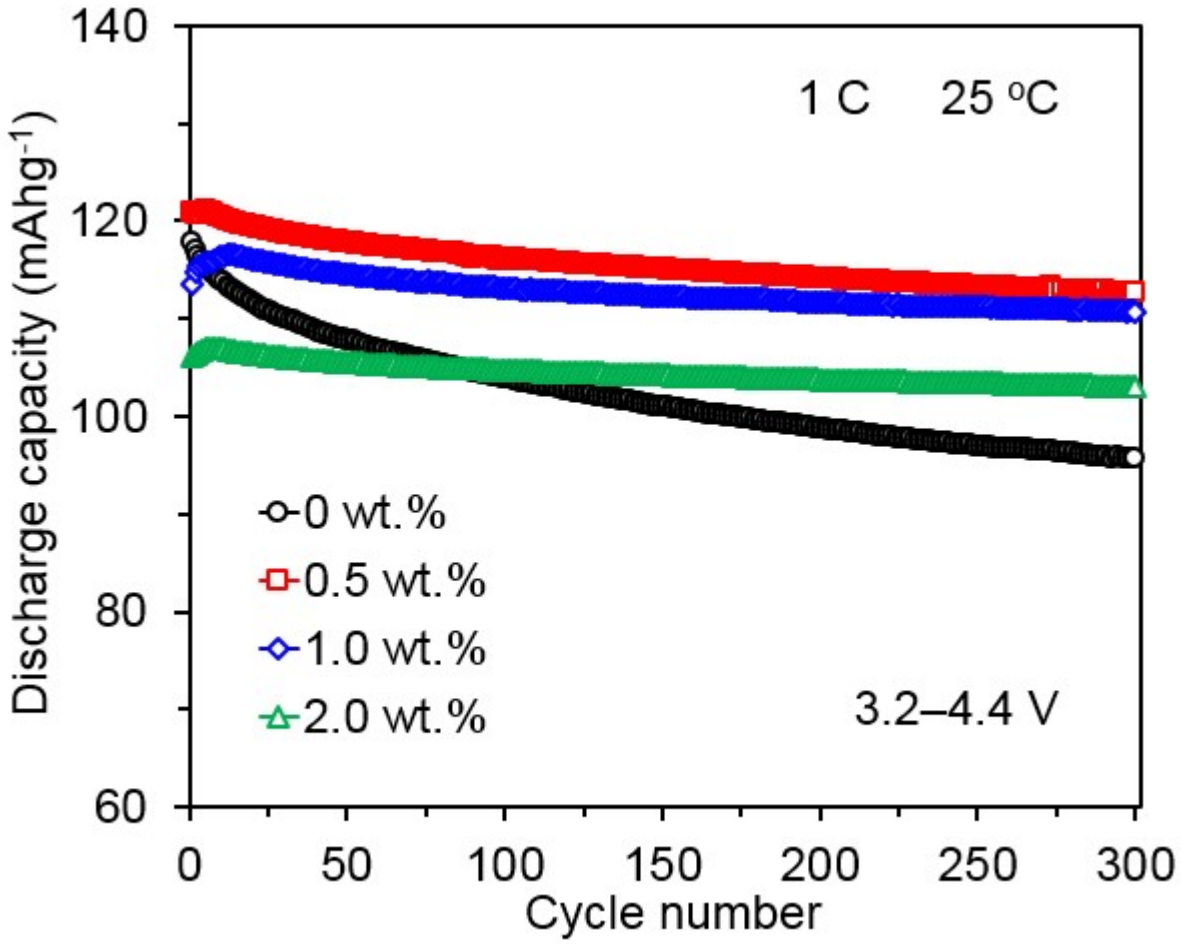
1 C 25 °C
Discharge capacity (mAhg-1)
Cycle number
0 wt.%
0.5 wt.%
1.0 wt.%
2.0 wt.%
3.2–4.4 V
140
120
100
80
60
0
50
100
150
200
250
300

Fig. 6

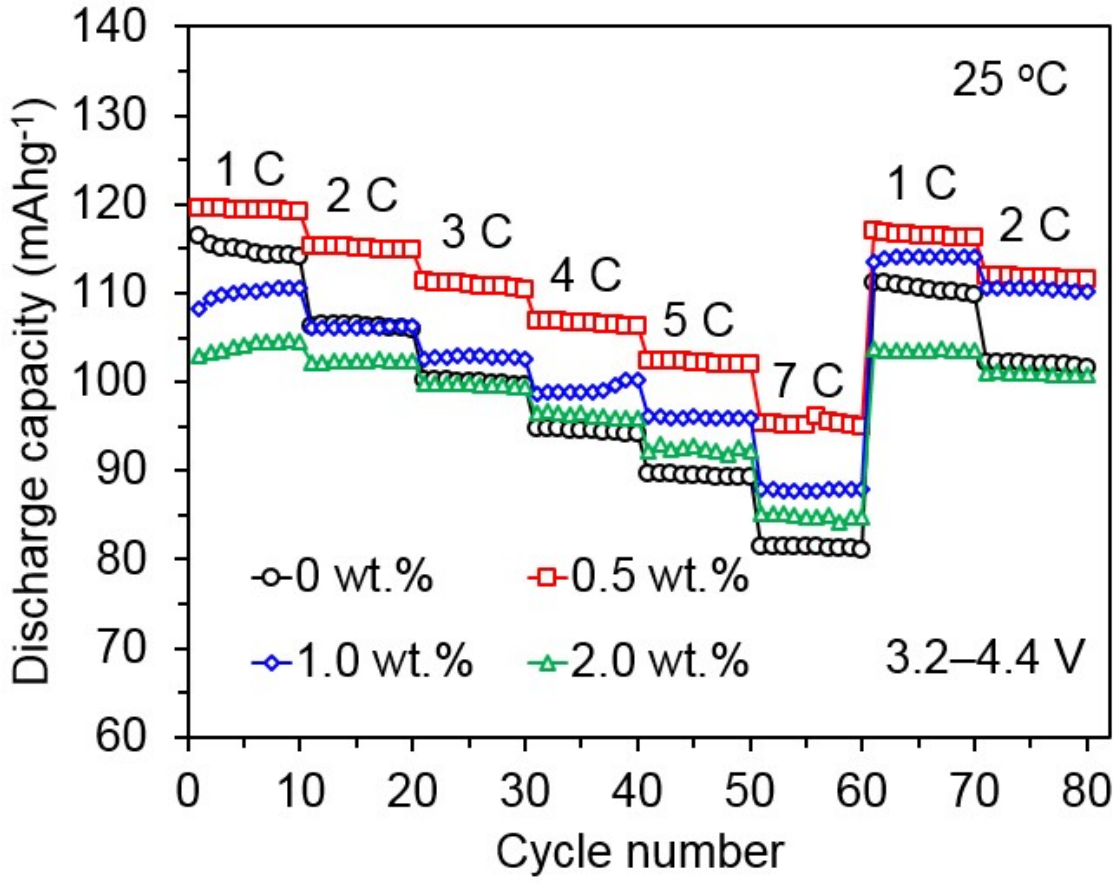
25 °C
1 C
2 C
3 C
4 C
5 C
7 C
1 C
2 C
0 wt.%
0.5 wt.%
1.0 wt.%
2.0 wt.%
3.2–4.4 V
Discharge capacity (mAhg-1)
Cycle number
140
130
120
110
100
90
80
70
60
0
10
20
30
40
50
60
70
80

Fig. 7

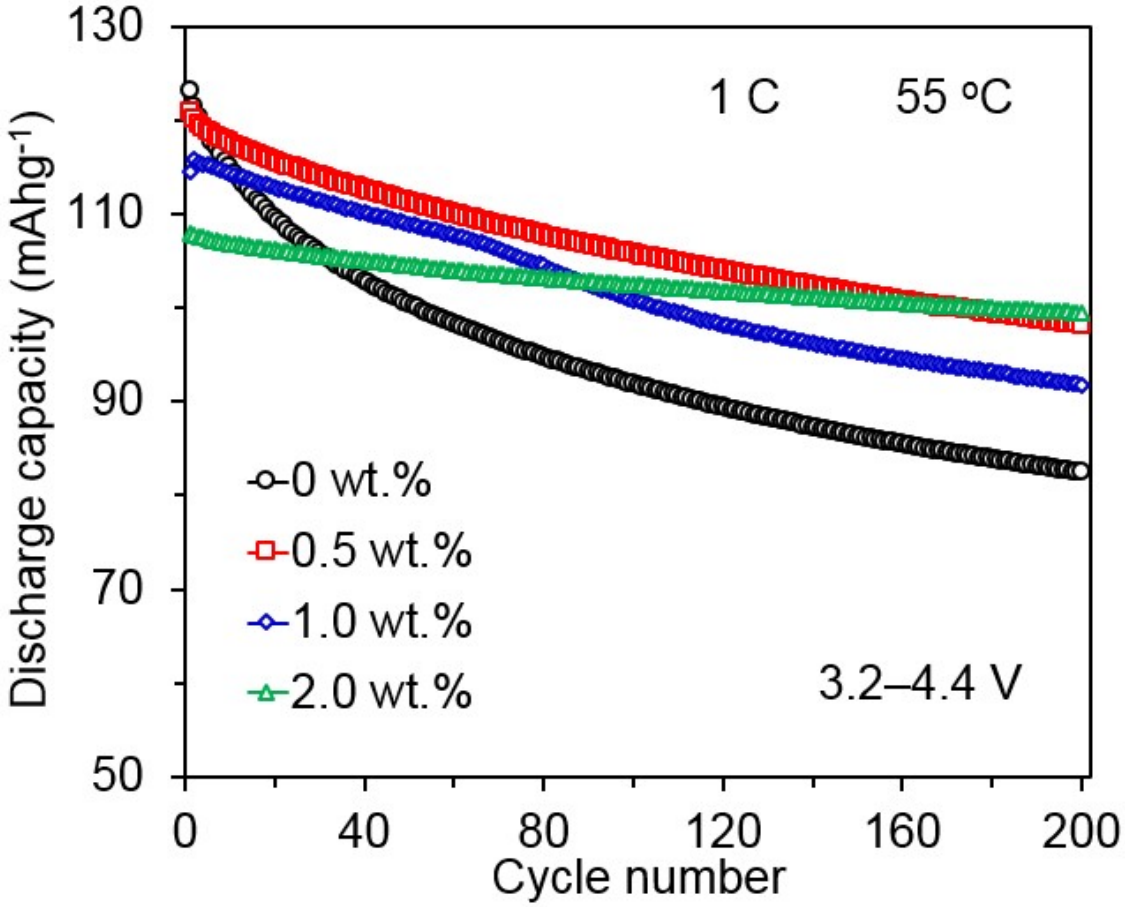
130
110
90
70
50
Discharge capacity (mAhg-1)
1 C
55 °C
0 wt.%
0.5 wt.%
1.0 wt.%
2.0 wt.%
3.2–4.4 V
0
40
80
120
160
200
Cycle number

Fig. 8

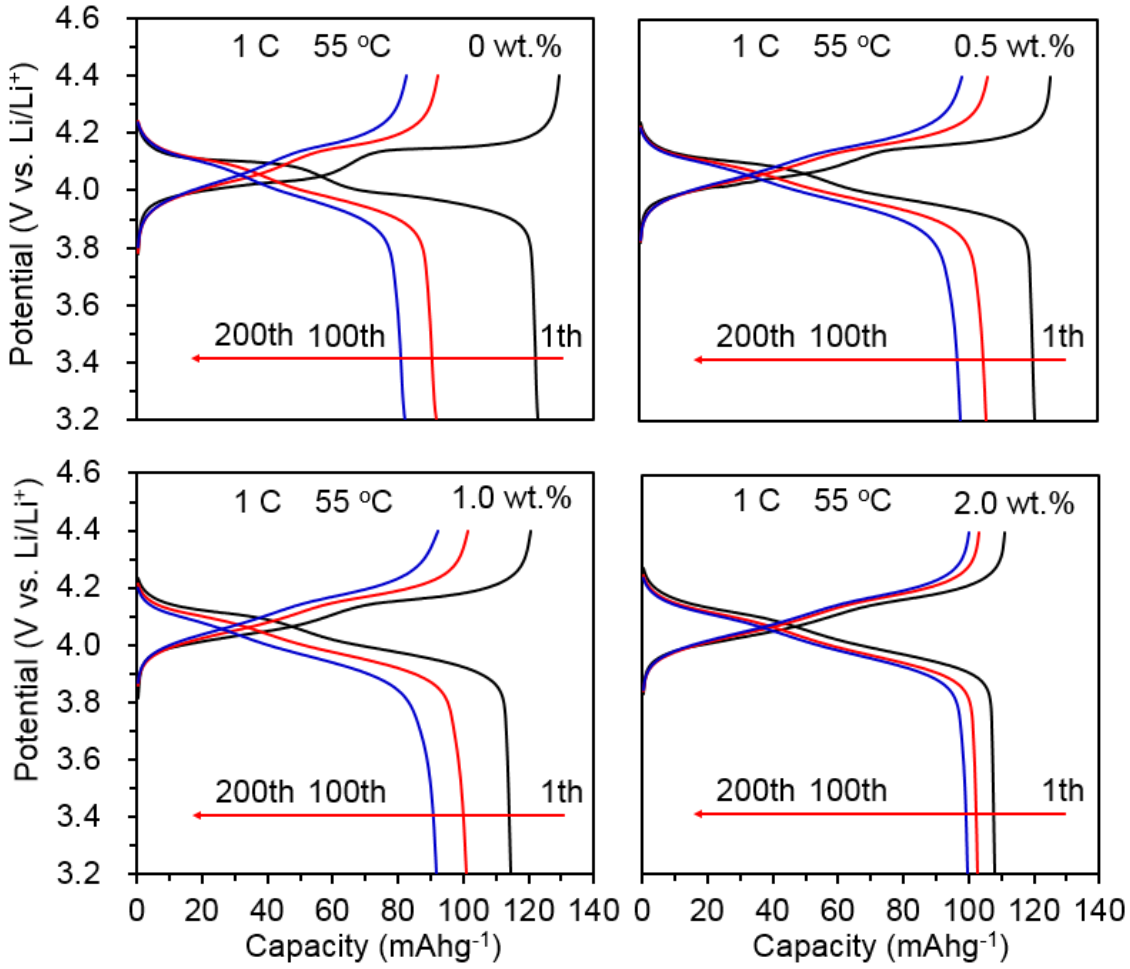
1 C 55 °C 0 wt.%
1 C 55 °C 0.5 wt.%
1 C 55 °C 1.0 wt.%
1 C 55 °C 2.0 wt.%
200th 100th 1th
Potential (V vs. Li/Li+)
Capacity (mAhg-1)
4.6
4.4
4.2
4.0
3.8
3.6
3.4
3.2
0 20 40 60 80 100 120 140

Fig. 9

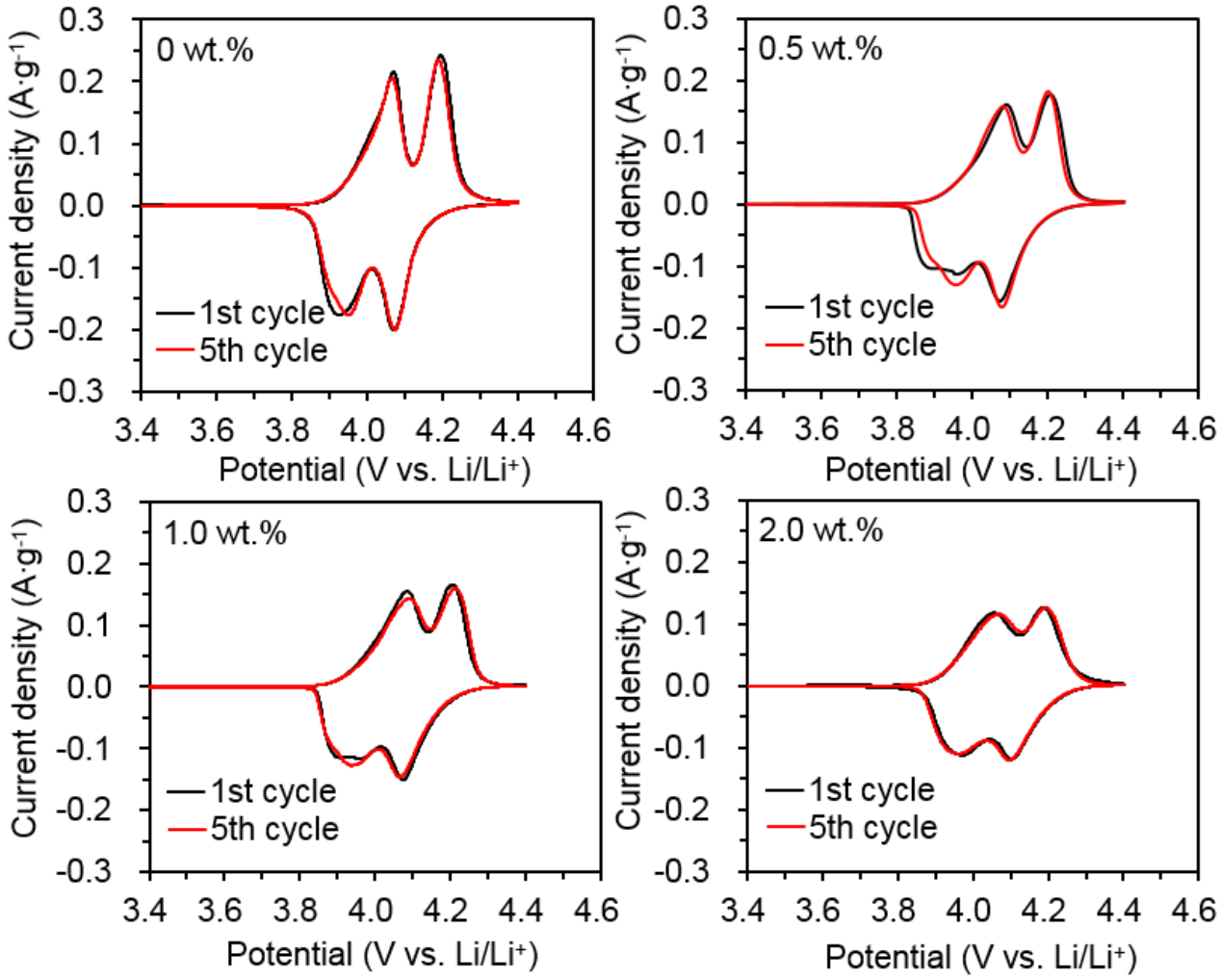
0 wt.%
0.5 wt.%
1.0 wt.%
2.0 wt.%
1st cycle
5th cycle
Current density (A·g⁻¹)
Potential (V vs. Li/Li⁺)
0.3
0.2
0.1
0.0
-0.1
-0.2
-0.3
3.4
3.6
3.8
4.0
4.2
4.4
4.6

Fig. 10

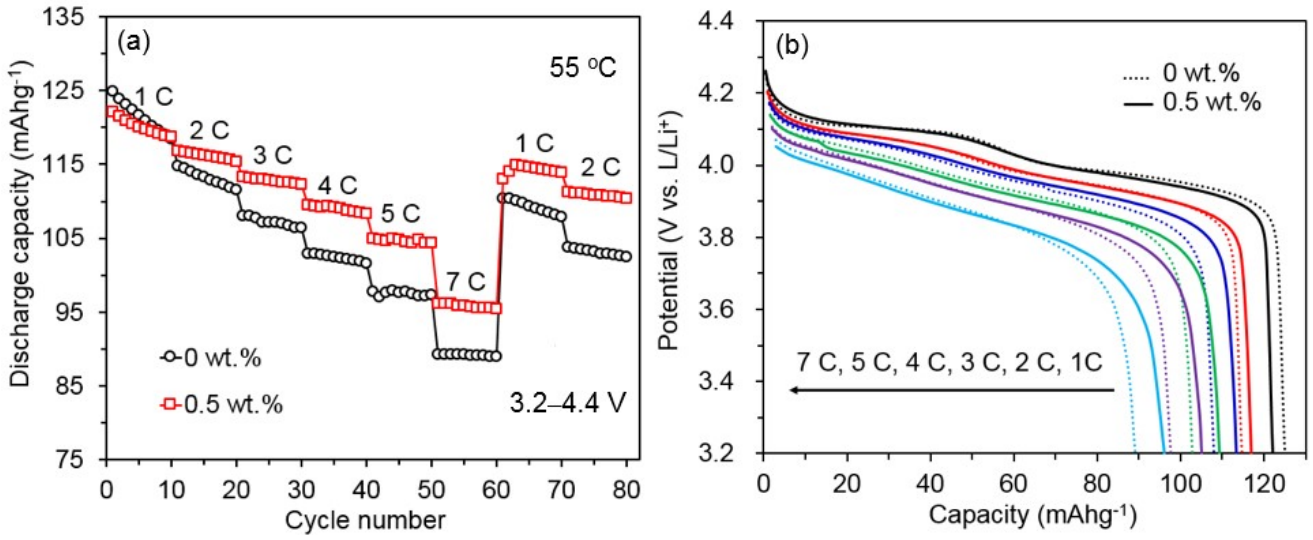
(a)
55 °C
1 C
2 C
3 C
4 C
5 C
7 C
1 C
2 C
0 wt.%
0.5 wt.%
3.2–4.4 V
Discharge capacity (mAhg-1)
Cycle number
(b)
0 wt.%
0.5 wt.%
7 C, 5 C, 4 C, 3 C, 2 C, 1C
Potential (V vs. L/Li+)
Capacity (mAhg-1)

Fig. 11

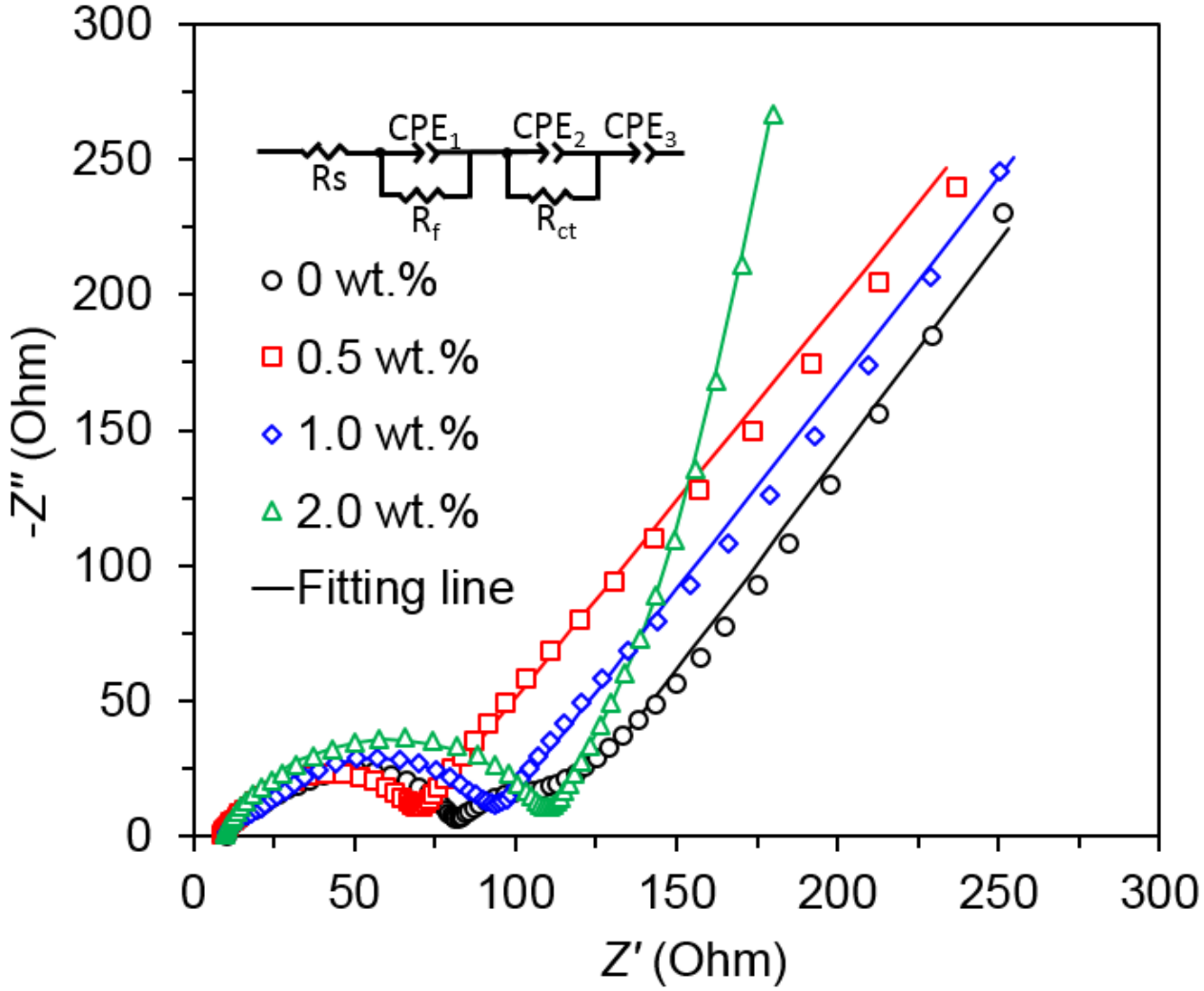
300
250
200
150
100
50
0
-Z'' (Ohm)
0
50
100
150
200
250
300
Z' (Ohm)
CPE1
CPE2
CPE3
Rs
Rf
Rct
0 wt.%
0.5 wt.%
1.0 wt.%
2.0 wt.%
Fitting line

Fig. 12

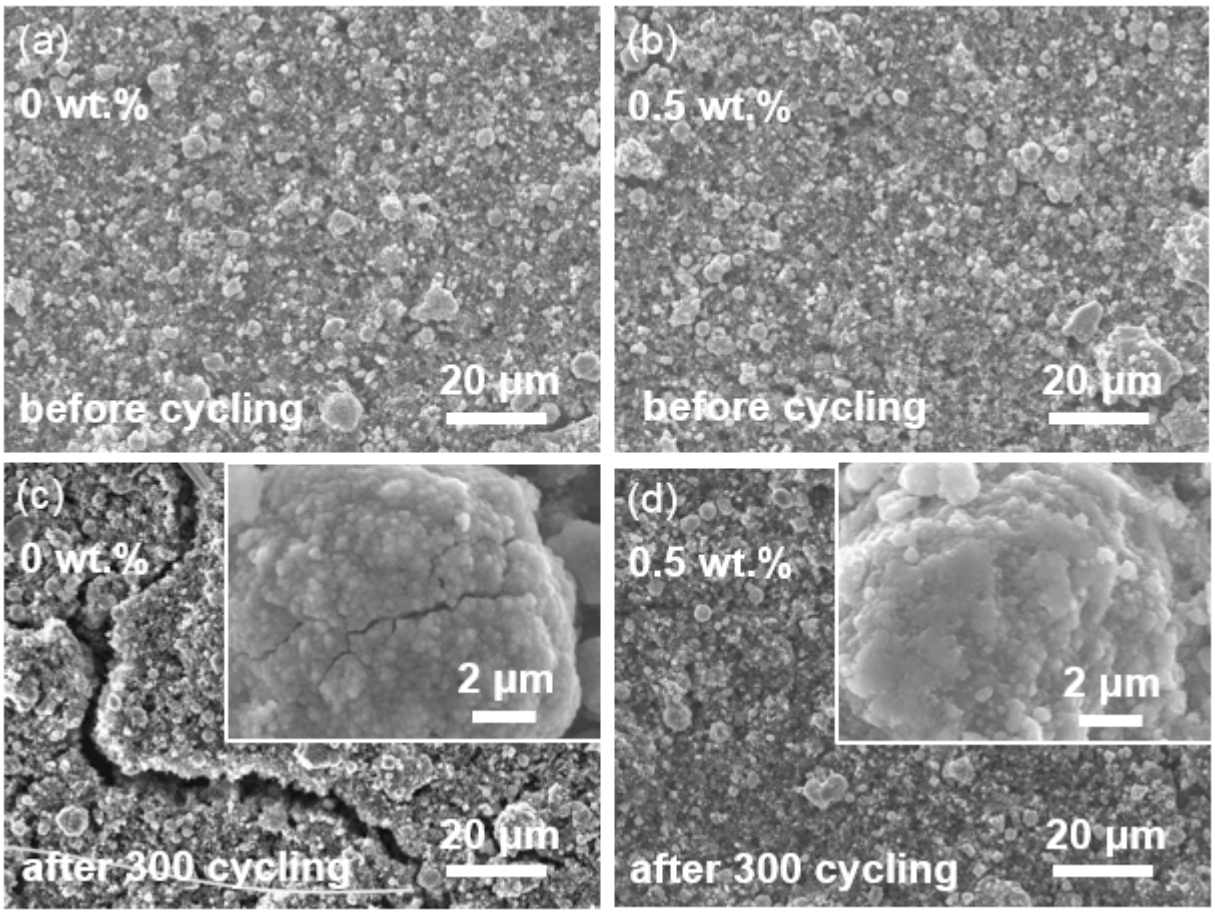
(a)
0 wt.%
before cycling
20 μm
(b)
0.5 wt.%
before cycling
20 μm
(c)
0 wt.%
2 μm
after 300 cycling
20 μm
(d)
0.5 wt.%
2 μm
after 300 cycling
20 μm

Table 1. Lattice parameters and cell volumes for modified $LiMn_2O_4$ samples.

Sample	*a* (Å)	Cell volume ($Å^3$)
0 wt.%	8.2406	559.60
0.5 wt.%	8.2350	558.46
1.0 wt.%	8.2316	557.77
2.0 wt.%	8.2230	556.02

Table 2. Potential values at the first cycle for modified $LiMn_2O_4$ samples.

Sample	E_{pa1} (V)	E_{pa2} (V)	E_{pc1} (V)	E_{pc2} (V)	ΔE_{p1} (V)	ΔE_{p2} (V)
0 wt.%	4.07	4.20	3.93	4.06	0.14	0.14
0.5 wt.%	4.08	4.21	3.96	4.07	0.12	0.14
1.0 wt.%	4.08	4.20	3.96	4.08	0.12	0.12
2.0 wt.%	4.05	4.18	3.97	4.10	0.08	0.08

ΔE_p represents the separation between the anodic peak potential, $E_{pa,}$ and the cathodic peak potential, E_{pc}.

Table 3. EIS parameters obtained from the fitted curves using the equivalent circuit shown in Fig. 11. All data are based on electrode of cm^{-2}, and the units of R and CPE are Ω and $S \cdot sec^n$, respectively.

Sample	R_s	R_f	CPE_1	n_1	R_{ct}	CPE_2	n_2	CPE_3	n_3
0 wt.%	9.91	27.01	1.66×10^{-3}	0.87	75.60	1.20×10^{-5}	0.68	1.34×10^{-2}	0.64
	± 0.03	± 0.21	± 0.47	± 0.16	± 0.03	± 0.18	± 0.02	± 0.05	± 0.04
0.5	9.24	6.59	1.08×10^{-6}	0.96	49.23	2.61×10^{-6}	0.92	1.32×10^{-3}	0.62
wt.%	± 0.02	± 0.33	± 0.99	± 0.09	± 0.05	± 0.22	± 0.03	± 0.01	± 0.01
1.0	10.90	9.03	2.74×10^{-7}	0.99	70.31	4.21×10^{-6}	0.85	1.81×10^{-3}	0.63
wt.%	± 0.02	± 0.15	± 0.71	± 0.06	± 0.03	± 0.17	± 0.02	± 0.01	± 0.01
2.0	9.14	26.13	2.43×10^{-3}	0.86	103.30	5.51×10^{-6}	0.77	1.24×10^{-3}	0.90
wt.%	± 0.02	± 0.61	± 0.59	± 0.22	± 0.02	± 0.09	± 0.01	± 0.02	± 0.03